# Supplementary Information for 'Fragility of the Dirac Cone Splitting in Topological Crystalline Insulator Heterostructures'

Craig M. Polley,[1,*] Ryszard Buczko,[2] Alexander Forsman,[3] Piotr Dziawa,[2] Andrzej Szczerbakow,[2] Rafał Rechciński,[2] Bogdan J. Kowalski,[2] Tomasz Story,[2] Małgorzata Trzyna,[4] Marco Bianchi,[5] Antonija Grubišić Čabo,[5] Philip Hofmann,[5] Oscar Tjernberg,[3] and Thiagarajan Balasubramanian[1]

[1] *MAX IV Laboratory, Lund University, 221 00 Lund, Sweden*
[2] *Institute of Physics, Polish Academy of Sciences, 02-668 Warsaw, Poland*
[3] *KTH Royal Institute of Technology, SCI Materials Physics, S-164 40 Kista, Sweden*
[4] *Center for Microelectronics and Nanotechnology, Rzeszow University, Rejtana 16A, Rzeszow 35-959, Poland*
[5] *Department of Physics and Astronomy, Interdisciplinary Nanoscience Center (iNANO), Aarhus University, 8000 Aarhus C, Denmark*

## I. DIRAC POINT VALLEY SPLITTING IN THE PRESENCE OF SURFACE TERRACES

The (001) surface of $Pb_{1-x}Sn_xSe$ breaks the symmetry of translation along the [001] direction, permitting the existence of surface states composed of the contributions from two $L$ valleys at the $L_1 = (1,1,1)\frac{\pi}{a_0}$ and $L_2 = (1,1,-1)\frac{\pi}{a_0}$ points in the bulk Brillouin zone.

Let us assume that we know the solutions of the effective mass equation for the nontrivial surface or interface states obtained only for one valley $L_1$. We restrict our consideration only to the solution at $\overline{X}$ in the surface Brillouin zone, and to eigenstates of the $(1\bar{1}0)$ mirror plane which correspond to eigenvalue $M = -i$. After omitting quadratic $k$ terms in the Hamiltonian, one can obtain a wavefunction of the form:

$$F_1(\overrightarrow{r}) = e^{i\varphi} f(z)(a\Psi_1^+(\overrightarrow{r}) + b\Psi_1^-(\overrightarrow{r})) \tag{1}$$

where $a$ and $b$ are real and $\Psi_1^{\pm}$ are the Bloch functions transforming according to $L_6^+$ and $L_6^-$ irreducible representations of the $D_{3d}$ point group, as known for IV-VI semiconductors. The envelope real function $f(z)$ is exponentially decaying for $z \to \infty$ (substrate bulk region). The phase $\varphi$, in the general case of an anisotropic effective mass, depends on $z$ and is defined up to an arbitrary phase $\varphi_0$.

The appropriate wavefunction for the $L_2$ valley can be obtained by time reversal symmetry $\Theta$ followed by the $\pi$ rotation $C_2$ around the [110] axis.

$$F_2(\overrightarrow{r}) = C_2\Theta F_1(\overrightarrow{r}) = e^{-i\varphi} f(z)(a\Psi_2^+(\overrightarrow{r}) + b\Psi_2^-(\overrightarrow{r})) \tag{2}$$

The valley mixing effect can be described by a simple model proposed by Liu[1], where the zero order mixing operator in the $M = -i$ subspace is given by:

$$\Delta = m\tau_x + \delta\tau_y \tag{3}$$

Within this model the antibonding and bonding superpositions of $F_i$ are:

$$F_{\pm} = (F_1 \pm e^{i\chi}F_2)/\sqrt{2} \tag{4}$$

where $\chi = \arg(m + i\delta)$. The phase $\varphi_0$ is no more arbitrary, because it alters the phase difference between two components in $F_{\pm}$, and we have assumed that $\varphi_0 = 0$ for above special solutions corresponding to two Dirac points. The valley splitting is given by $2\sqrt{m^2+\delta^2}$.

The $\Psi_{1,2}^{\pm}$ Bloch wavefunctions in equations 1,2 are combinations of the Bloch sums defined by atomic-like (Löwdin) orbitals:

$$\Psi_i^{\pm} = \sum_{\alpha} c_{\alpha,i}^{\pm}\Phi_{\alpha,i} \tag{5}$$

where $\alpha$ denotes cation or anion orbitals associated with the appropriate spin aligned in the direction perpendicular to the mirror plane $(1,-1,0)$, and

$$\Phi_{\alpha,i}(\overrightarrow{r}) = \frac{1}{\sqrt{N}} \sum_{\overrightarrow{t}} e^{i\overrightarrow{L}_i(\overrightarrow{t}+\overrightarrow{d})} \phi_\alpha(\overrightarrow{r} - \overrightarrow{t} - \overrightarrow{d}) \tag{6}$$

The translation vectors $\overrightarrow{t} = l\overrightarrow{t_1} + m\overrightarrow{t_2} + n\overrightarrow{t_3}$ are based on the primitive lattice translation vectors:
$\overrightarrow{t_1} = (1,-1,0)\frac{a_0}{2}$, $\overrightarrow{t_2} = (1,1,0)\frac{a_0}{2}$ and $\overrightarrow{t_3} = (1,0,1)\frac{a_0}{2}$.
Note that $\overrightarrow{t_1}$ and $\overrightarrow{t_2}$ are parallel to (001) surface.

The displacement vectors $\overrightarrow{d}$ are fixed offsets according to the lattice structure: $\overrightarrow{d} = 0$ for cation and $\overrightarrow{d} = (100)\frac{a_0}{2}$ for anion atom positions.

Rather than using the $\Phi_{\alpha,i}$ basis, it is more convenient to work with combinations:

$$\Phi_{\alpha,+} = (\Phi_{\alpha,1} + \Phi_{\alpha,2})/\sqrt{2}, \qquad \Phi_{\alpha,-} = (\Phi_{\alpha,1} - \Phi_{\alpha,2})/\sqrt{2} \tag{7}$$

The appropriate Bloch sums are now:

$$\begin{aligned}
\Phi_{\alpha,+}(\overrightarrow{r}) &= \frac{1}{\sqrt{N}} \sum_{l,m} (-1)^m \sum_j \phi_\alpha(\overrightarrow{r} - l\overrightarrow{t_1} - m\overrightarrow{t_2} - 2j\overrightarrow{t_3} - \overrightarrow{d}) \\
\Phi_{\alpha,-}(\overrightarrow{r}) &= \frac{-1}{\sqrt{N}} \sum_{l,m} (-1)^m \sum_j \phi_\alpha(\overrightarrow{r} - l\overrightarrow{t_1} - m\overrightarrow{t_2} - (2j+1)\overrightarrow{t_3} - \overrightarrow{d})
\end{aligned} \tag{8}$$

An important aspect of the above sums is that they are combinations of orbitals centered at every second atomic plane, as a direct consequence of the fact that the $L$ point separation is equal to $2\pi/a_0[0,0,1]$. If we define the index $j$ as equal to one at the (001) surface plane, then $\Phi_-$ is defined by atoms at the surface and all odd numbered atomic planes, whereas $\Phi_+$ contains atoms situated in even numbered planes.

After covering the surface with a new atomic layer, the role of $\Phi_-$ and $\Phi_+$ is exchanged. Now, with $j$ starting from 0 in the sums, $\Phi_+$ is defined by surface atoms and $\Phi_-$ by atoms in the next layer. It can be shown that also the antibonding and bonding character of $F_\pm$ combinations is exchanged, and valley splitting remains unaffected. It should be noticed that the exchange of $F_\pm$ character can be also achieved by changing $\varphi_0$ to $\pi/2$, which leads a change of the total phase difference between two $L$ valley components by $\pi$.

In the case of a surface covered by a sufficiently dense array of terraces or steps, the $\varphi_0$ remains fixed across the entire surface. But since odd-height regions cancel the valley interactions produced by surface and even-height regions, the overall effect will be a cancellation of the valley splitting, dependent on the ratio of odd- to even-height regions on the surface. In the case of terraces made from the same atoms as the substrate (e.g. homoepitaxial growth), total cancellation should occur for half coverage of odd-height terraces. When terraces are made with different material, the assumption typically used in effective mass theory of identical Bloch functions across the entire structure is not well satisfied, and the coverage for total cancellation can differ from 1/2.

Each of the $F_\pm$ solutions is constructed with Bloch sums corresponding to even and odd atomic layers, however for a given orbital $\alpha$ the contributions of $\Phi_{\alpha,-}$ and $\Phi_{\alpha,+}$ are not the same. They depend on $\alpha$ and are opposite for bonding and antibonding states. As a result $F_\pm$ wavefunctions rapidly oscillate in antiphase and with two atomic layer periodicity, as shown in Fig. 5d. This leads to another form of valley splitting oscillation with overlayer thickness when the wavefunctions are localized at the interface between a TCI and normal insulator and the surface layer is always fully completed.

## II. SUPPORTING EXPERIMENTS

In Figs.1-3 we summarize additional sample preparations and measurements. While the growth conditions were broadly similar to those employed in the main manuscript, these measurements lack a reliable thickness characterization. While a comparable growth rate is expected (2 ML $min^{-1}$), we specify only the PbSe deposition time. These measurements demonstrate that the changes in Dirac cone splitting are reproducible. All spectra were acquired with p-polarized photons, with photon energies of 18 eV (ARPES) or 90 eV (core levels).

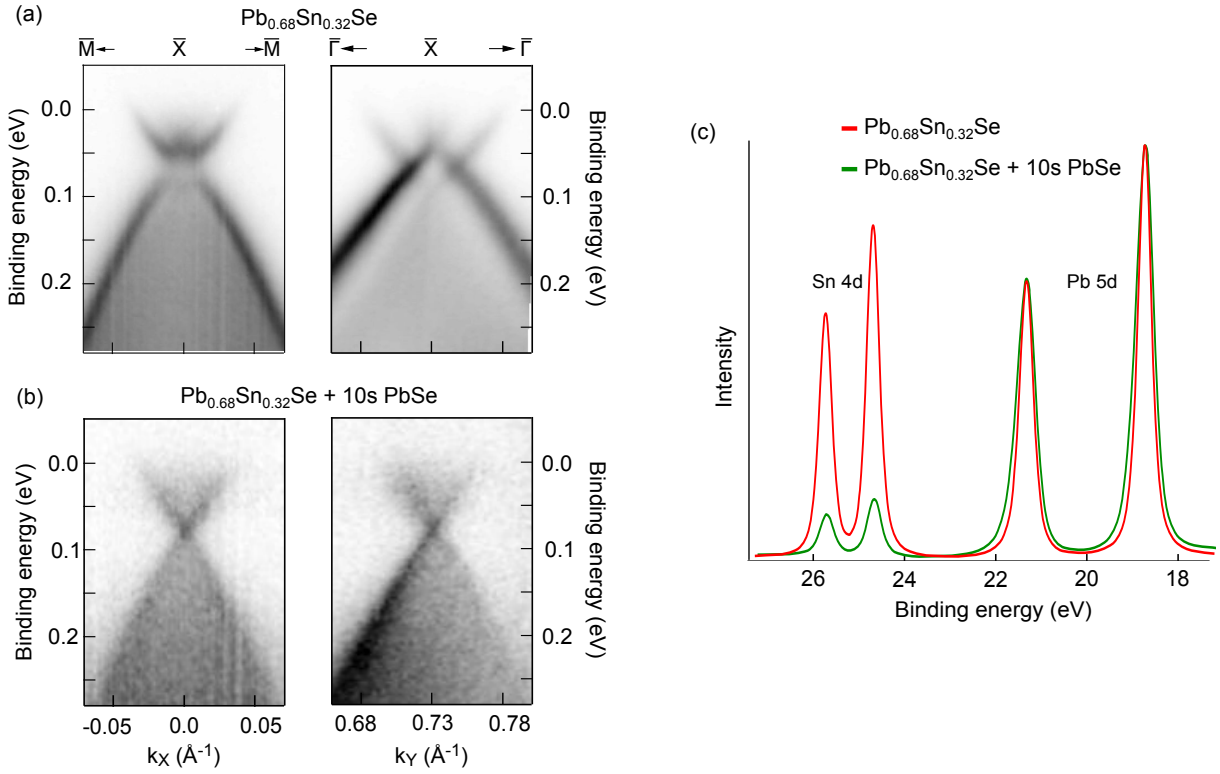


FIG. 1. **Measurements taken at the i4 beamline at the MAX-IV facility on a substrate with slightly higher Sn content (x=0.32), confirming the collapse of the valley splitting after PbSe deposition. The sample temperature was maintained at ≈130 K during measurements using a bath liquid nitrogen cryostat.**

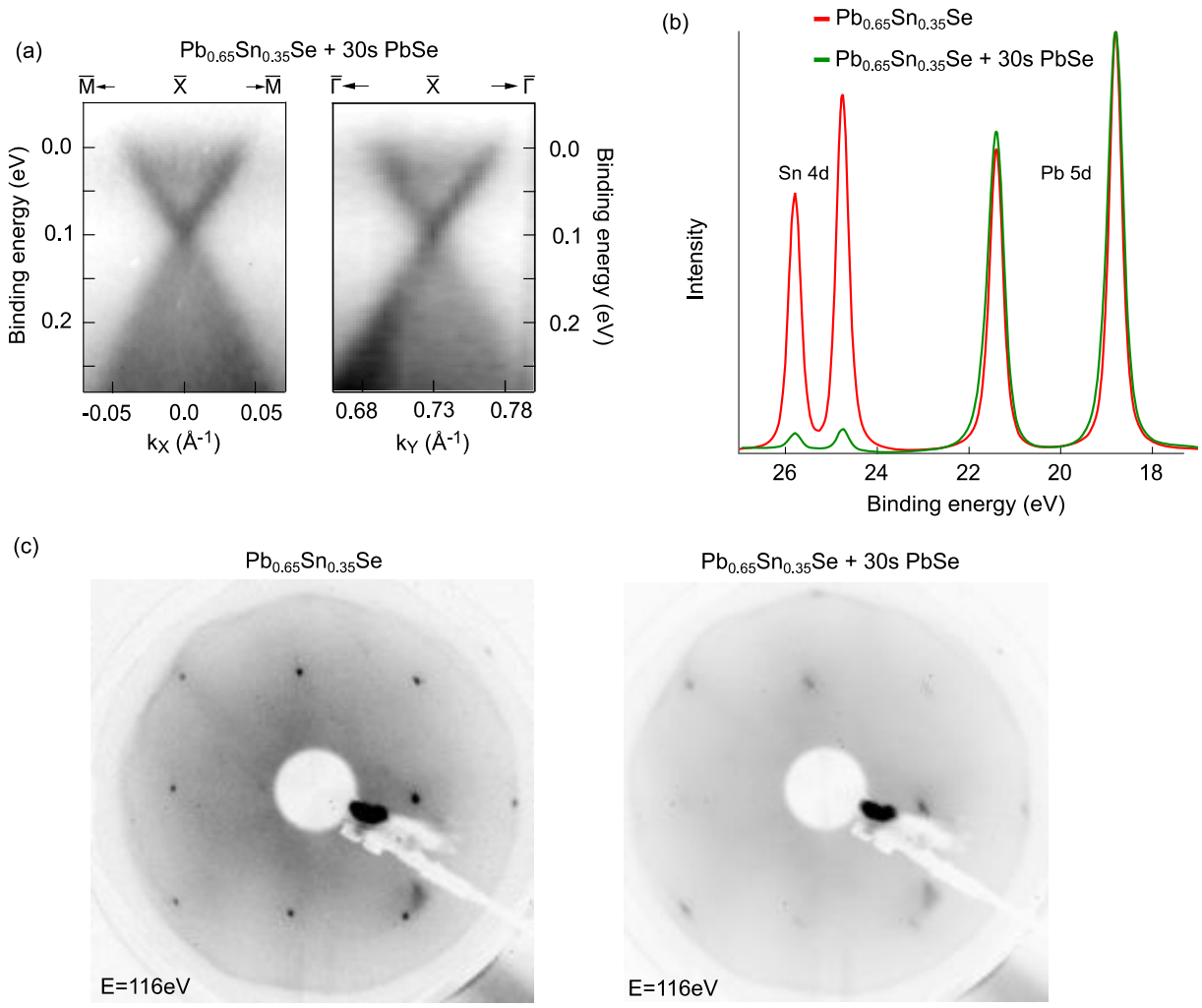


FIG. 2. **Measurements taken at the i4 beamline at the MAX-IV facility on a substrate with slightly higher Sn content (x=0.35), confirming the collapse of the valley splitting. The sample temperature was maintained at ≈130 K during measurements using a bath liquid nitrogen cryostat. LEED measurements before and after PbSe deposition (c) demonstrate that the PbSe overlayer retains the (001) orientation of the substrate without reconstruction.**

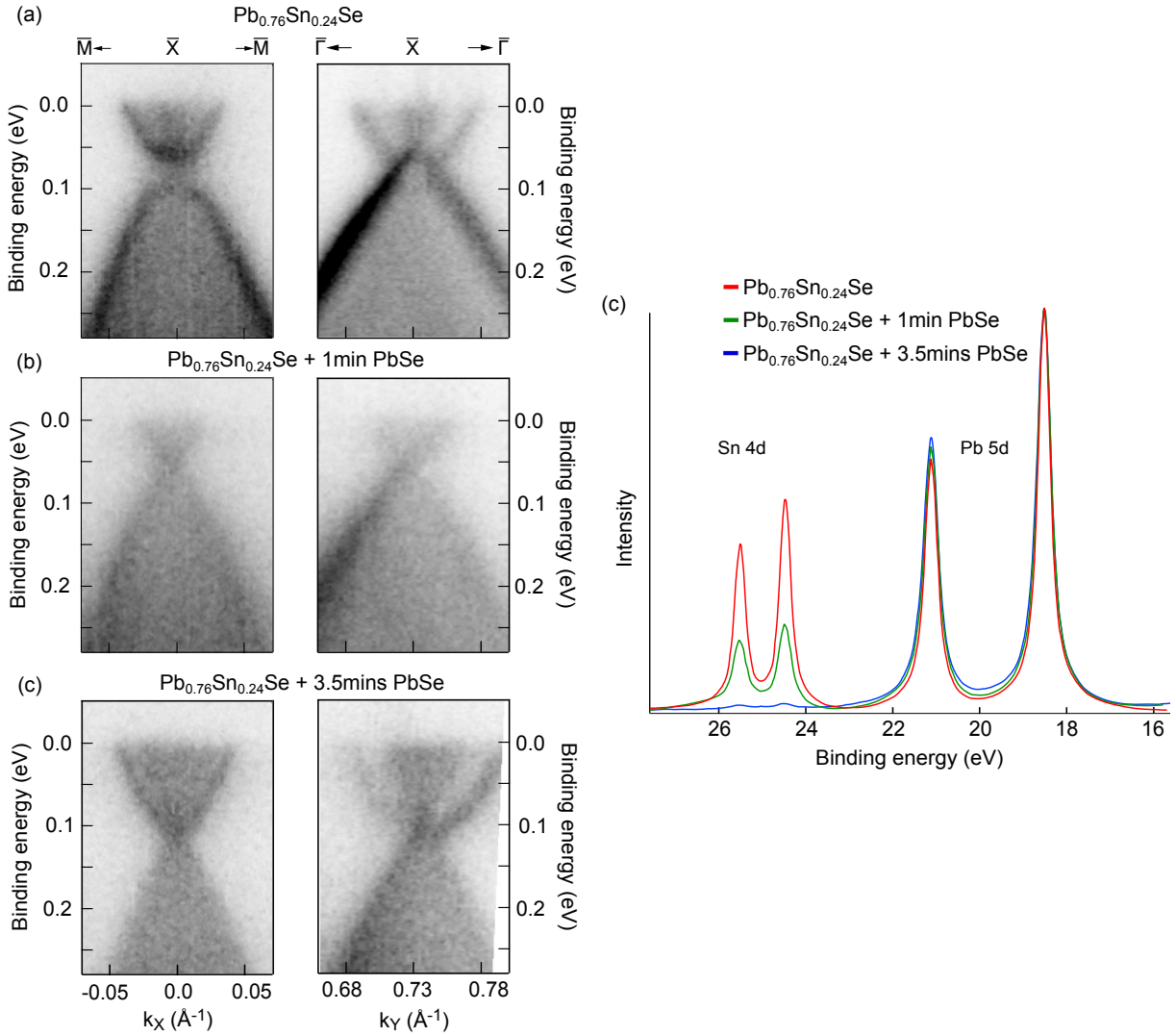


FIG. 3. **Measurements taken at the SGM-3 beamline at the ASTRID 2 facility on a substrate with lower Sn content (x=0.24), confirming the oscillatory changes with thickness. PbSe growth was performed with the same PbSe source but with higher substrate temperatures (≈70°C). The sample temperature was maintained at ≈16 K during measurements using a liquid helium cryostat.**

## III. $k \cdot p$ FITTING AND CHANGES IN DISPERSION

On the clean surface the two parent Dirac cones have identical $k_{\parallel}$ dispersion, but careful inspection reveals that this is not the case after 3.9 ML of PbSe deposition (Fig. 4g). Such behaviour is included in the symmetry derived $k \cdot p$ model of Liu[1], provided we include higher order terms:

$$H(k) = (v_x k_x s_y - v_y k_y s_x) + (v'_x k_x s_y - v'_y k_y s_x)\tau_x + m\tau_x + \delta s_x \tau_y \quad (9)$$

Here $x$ is the $\bar{X}$-$\bar{M}$ direction and $y$ the $\bar{X}$-$\bar{\Gamma}$ direction. The parameter $v$ is the band velocity, modified for each parent cone by $v'$ (one becomes $v + v'$, the other $v - v'$), $m$ is the energy splitting of the parent Dirac cones at $k = \bar{X}$ and $\delta$ is the hybridization strength between the parent Dirac cones outside of the mirror symmetry protected $\bar{\Gamma}$-$\bar{X}$-$\bar{\Gamma}$ plane. The matrices $s$ and $\tau$ are Pauli matrices in spin and valley space. All but the first two terms in Eqn. 9 are off-diagonal in valley space (through $\tau_x$ and $\tau_y$), and thus introduce effects of intervalley interactions.

This expanded Hamiltonian can be solved numerically for the band dispersions, but rigorously fitting our experimental data with this model is not straightforward. The real spectra contain diffuse intensity from other sources such as scattering from nearby bulk bands, which the 4-band $k \cdot p$ model does not describe. In Table I we summarize our best estimates of the $k \cdot p$ parameters for the three clearest datasets. Peak positions extracted from momentum and electron distribution curves yield the band velocity parameters $v$ and $v'$, and by extrapolation a first estimate of the energy gap $\Delta$. A non-zero hybridization term $\delta$ results in bending of the bands which slightly enlarges the apparent energy splitting $m$. This coupling implies that it is insufficient to analyze only a $\bar{\Gamma}$-$\bar{X}$-$\bar{\Gamma}$ image. In addition, when $m$=0 no band crossings occur outside of the mirror plane, so $\delta$ cannot be extracted. Here we determine $m$ and $\delta$ by iteratively calculating the band dispersion and comparing the output to the $\bar{M}$-$\bar{X}$-$\bar{M}$ and $\bar{\Gamma}$-$\bar{X}$-$\bar{\Gamma}$ spectra.

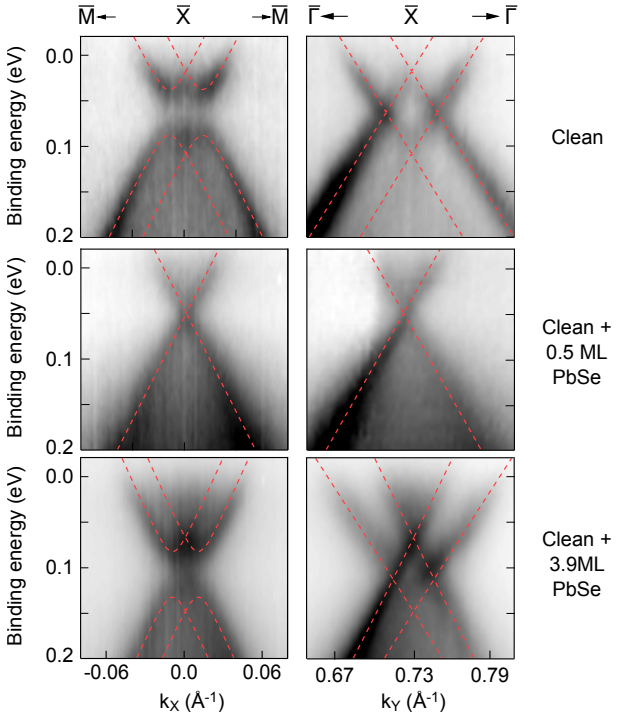


FIG. 4. **Theoretical description of the $k_{//}$ dispersions. Applying the symmetry derived $k \cdot p$ model model of Liu[1] (red dashed lines) using empirically determined parameters listed in Table I captures the evolving behaviour of the interface state bandstructure.**

With very little PbSe coverage, the inter-valley interactions appear to vanish. The resulting band dispersion is nearly isotropic, which can be understood from consideration of the bulk bandstructure. In contrast to (Pb,Sn)Te, the bulk conduction and valence bands in (Pb,Sn)Se have nearly isotropic effective masses. With respect to the major axis along the [111] direction, the effective mass anisotropy $\frac{m_{\parallel}}{m_{\perp}}$ begins at 1.7 for PbSe and approaches unity for Sn contents >0.2[2]. Since these ellipsoids are tilted with respect to the (001) surface, the surface state effective mass anisotropy is further reduced to $\frac{1}{3}(2 + m_{\parallel}/m_{\perp})$[3].

Changes in the valley splitting term $m$ have already been discussed, but the non-zero $v'_y$ for the 3.9 ML sample warrants further comment. A band velocity adjustment could equivalently be interpreted as a $k_{\parallel}$-dependent valley

| PbSe depth (ML) | $v_x$ (eVÅ) | $v_y$ (eVÅ) | $v'_x$ (eVÅ) | $v'_y$ (eVÅ) | $m$ (meV) | $\delta$ (meV) |
|---|---|---|---|---|---|---|
| 0 | 2.9 | 2.3 | 0 | 0 | 76 | 25 |
| 0.5 | 2.8 | 2.5 | 0 | 0 | 0 | – |
| 3.9 | 3.2 | 2.6 | 0 | 0.4 | 64 | 25 |

TABLE I. Parameters used in the $k \cdot p$ model to generate the curves in Figure 4.

splitting term. Since there have been no momentum-resolved experimental probes of valley splitting phenomena until very recently[4], momentum dependence has had limited theoretical consideration[5,6]. Since the interface state wavefunction is composed from the set of bulk Bloch states with the same $k_\parallel$, it is straightforward to see that changing $k_\parallel$ could modify this set and hence the valley splitting of the interface states.

## IV. CORE LEVEL ANALYSIS DETAILS

At each PbSe depth, the Pb 5d and Sn 4d core level spectra were acquired with identical spectrometer settings. Peak fitting was performed with a single Voigt doublet for each species separately, which allowed the Shirley background factor to differ. For the analysis performed in this study, the area of the background and of the peaks are the most important aspects; issues such as multiple components or minor binding energy offsets are of little consequence. The peak model was calculated iteratively as:

1. Generate a Gaussian convolved Lorentzian doublet
2. Compute an active Shirley background from this doublet[7]
3. Add a constant offset
4. Iterate until $\chi^2$ is minimized

**Estimating Sn fraction:** Peak areas $A$ were determined by numerically integrating the doublet from the fitting model (background subtracted). The tin fraction can then be estimated by:

$$x = \frac{(\frac{A}{\sigma})_{Sn4d}}{(\frac{A}{\sigma})_{Sn4d} + (\frac{A}{\sigma})_{Pb5d}} \tag{10}$$

Where the cross sections at h$\nu$=90 eV are $\sigma_{Sn4d}$=4.50 Mb and $\sigma_{Pb5d}$=5.17 Mb, obtained from Elettra's online "WebCrossSection" service which is based on the calculations of Yeh and Lindau[8]

**Estimating PbSe thickness:** On the clean $Pb_{0.7}Sn_{0.3}Se$ surface the photoemission intensity from the Sn 4d core level can be described as a summation over every slice in the vertical direction, attenuated according to the Beer-Lambert absorption law:

$$\begin{aligned} I_{Sn4d} &= K\sigma_{Sn4d}N_{Sn}\int_0^\infty \exp\Big(-\frac{z}{\lambda\cos\theta}\Big)dz \\ &= K\sigma_{Sn4d}N_{Sn}\lambda\cos\theta \end{aligned} \tag{11}$$

Where $K$ is a scaling factor based on experimental conditions such as photon flux, sample alignment and analyzer settings, $\sigma$ is the photoionization cross section, $N_{Sn}$ the planar atomic density of Sn atoms in $Pb_{0.7}Sn_{0.3}Se$, $z$ the distance into the substrate from the surface and $\lambda$ the inelastic mean free path of the photoelectron. Since the measurements are made at an angle $\theta$=23° away from normal emission (corresponding to $\bar{X}$ at h$\nu$=18 eV), the attenuation length is extended by the factor $\frac{1}{\cos\theta}$.

When a PbSe layer of thickness $d$ is deposited on the $Pb_{0.7}Sn_{0.3}Se$, this same total intensity from the Sn is now attenuated by having to travel through the PbSe layer:

$$I_{Sn4d}(d) = K\sigma_{Sn4d}N_{Sn}\lambda\exp\Big(-\frac{d}{\lambda cos(\theta)}\Big) \tag{12}$$

In practice the scaling factor $K$ differs between measurements, so that normalization is required. Here we normalize to the Pb 5d peak. On the clean $Pb_{0.7}Sn_{0.3}Se$ surface this has an intensity given by:

$$I_{Pb5d} = K\sigma_{Pb5d}N_{Pb}\lambda\cos\theta \tag{13}$$

The PbSe overlayer has a higher atomic density of Pb compared to $Pb_{0.7}Sn_{0.3}Se$, equivalent to the sum $(N_{Pb}+N_{Sn})$ in $Pb_{0.7}Sn_{0.3}Se$ (i.e. $1 = 0.7 + 0.3$). A simple way to incorporate this is to separate the overlayer contribution into that from $N_{Pb}$ and $N_{Sn}$ lead atoms, in which case we can write:

$$\begin{aligned} I_{Pb5d}(d) &= K\sigma_{Pb5d}N_{Pb}\lambda\cos\theta + K*\sigma_{Pb5d}N_{Sn}\int_0^d \exp\Big(-\frac{z}{\lambda\cos\theta}\Big)dz \\ &= K\sigma_{Pb5d}N_{Pb}\lambda\cos\theta + K\sigma_{Pb5d}N_{Sn}\lambda\cos\theta\left(1-\exp\Big(-\frac{d}{\lambda\cos\theta}\Big)\right) \end{aligned} \tag{14}$$

The depth dependent ratio of core level intensities $R(d)$ is given by:

$$\begin{aligned} R(d) &= \frac{I_{Pb5d}(d)}{I_{Sn4d}(d)} \\ &= \frac{\sigma_{Pb5d} N_{Pb}}{\sigma_{Sn4d} N_{Sn} \exp\left(-\frac{d}{\lambda cos(\theta)}\right)} + \frac{\sigma_{Pb5d}\left(1 - \exp\left(-\frac{d}{\lambda cos(\theta)}\right)\right)}{\sigma_{Sn4d} \exp\left(-\frac{d}{\lambda cos(\theta)}\right)} \\ &= \frac{R(0)}{\exp\left(-\frac{d}{\lambda cos(\theta)}\right)} + \frac{\sigma_{Pb5d}}{\sigma_{Sn4d}}\left(\exp\left(\frac{d}{\lambda cos(\theta)}\right) - 1\right) \end{aligned} \tag{15}$$

Since $R(d)$ is experimentally measured, we can determine the growth rate by fitting the above expression to our measurements (substituting (growth rate×time) for $d$). The inelastic mean free path in PbSe is not documented, but we expect it to be close to that of PbTe ($\lambda$=0.47 nm at $E_K$=63 eV, based on the "TPP-2M" formula of Tanuma, Powell and Pen[9,10]). As shown in Fig.5, this yields a growth rate of 0.08 Å$s^{-1}$. The rate determined by *ex-situ* electron microscopy should be considered more reliable, since the calculation here is strongly dependent on the parameter $\lambda$ and the accuracy of the TPP-2M result has not been quantified.

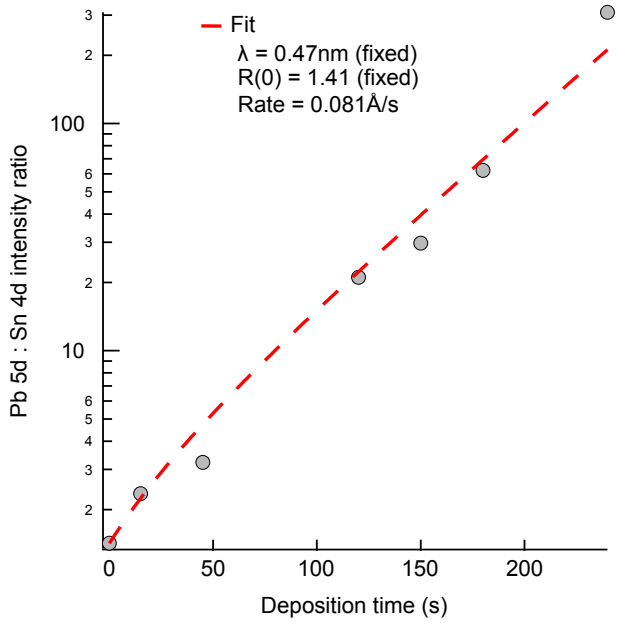


FIG. 5. **Fitting measured core level intensity ratios with Equation 15 to extract a PbSe growth rate estimate.**

## V. *EX-SITU* THICKNESS CALIBRATION

**Cross Sectional Electron Microscopy.** Immediately following the experiments described in the manuscript, PbSe was deposited on a clean $BaF_2$ substrate for 46 minutes. This gives a thick film which can easily be measured by *ex-situ* cross sectional electron microscopy (Fig.6). Examining 4 different images we obtain a film thickness of (28.7 ± 3.0) nm, equivalent to a growth rate of (0.10 ± 0.01) Ås$^{-1}$.

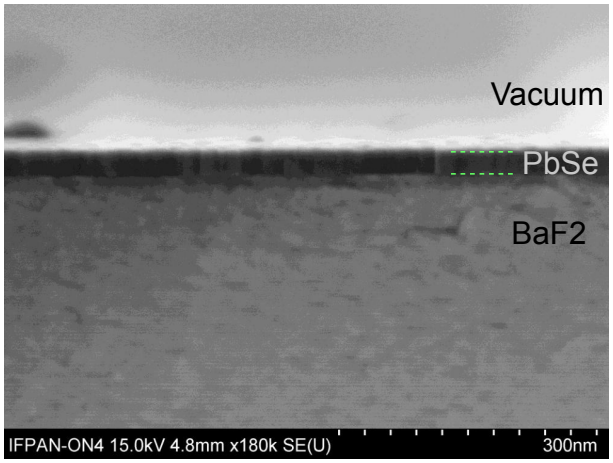


FIG. 6. **Example of a cross sectional electron microscopy image of the thick calibration film of PbSe on $BaF_2$.**

**Secondary Ion Mass Spectrometry.** Time-of-flight secondary ion mass spectrometry (TOF-SIMS) measurements were performed on the sample from which the ARPES in the manuscript was measured, using a TOF SIMS 5 (IONTOF GmbH, Münster, Germany) in dual beam mode. A $Bi^+$ primary beam (30 keV / 1.37 pA) and $Cs^+$ sputter beam (500 eV / 18 nA) were used in a non-interlaced mode. Positive secondary ions of $PbCs^+$, $SeCs^+$ and $SnCs^+$ were collected. The primary beam was rastered over an area of 100×100 $\mu m^2$, centered inside a sputter crater of 300×300 $\mu m^2$. The positive secondary ion mass spectra were calibrated using C, $CH_3^+$,$Sn^+$, $Se^+$, $Cs^+$ and $Cs_2^+$ Depth was calibrated based on crater depth, as measured by a DEKTAK stylus profilometer.

The interface positions were determined from the half maximum of the Pb and Se (front surface) and Sn (back surface) signals. This approach yields a film thickness of 9.4 nm, equivalent to a growth rate of 0.11 Ås$^{-1}$. The Sn signal drops sharply at the growth interface without obvious signs of segregation, in accordance with the photoemission analysis in the manuscript.

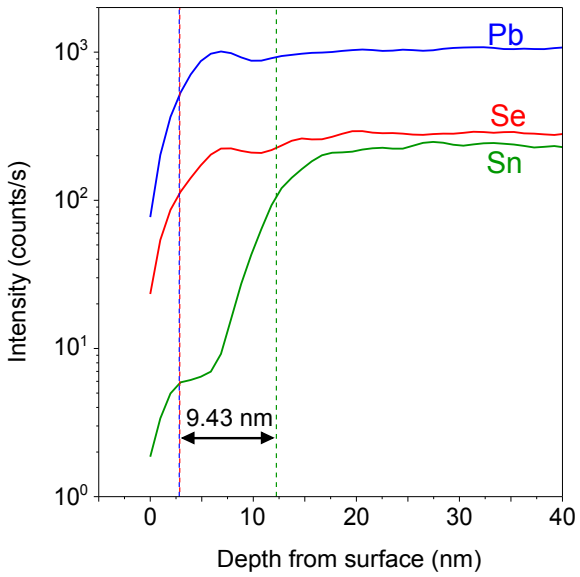


FIG. 7. **TOF-SIMS depth profiles of the Pb,Se and Sn species in the sample discussed in the manuscript.**

* craig.polley@gmail.com


[1] Liu, J.; Duan, W.; Fu, L. Two Types of Surface States in Topological Crystalline Insulators, *Phys. Rev. B* **2013**, *88* 241303(R)

[2] Nimtz, G.; Schlicht, B. in *Narrow-Gap Lead Salts* (ed. Höhler, G.) (Springer Tracts in Modern Physics, **1983** , *98*).

[3] Stern, F.; Howard, W. E. Properties of Semiconductor Surface Inversion Layers in the Electric Quantum Limit, *Phys. Rev.* **1967**, *163*, 816

[4] Miwa, J. A.; Warschkow, O.; Carter, D. J.; Marks, N. A.; Mazzola, F.; Simmons, M. Y.; Wells, J. W. Valley Splitting in a Silicon Quantum Device Platform, *Nano Letters* **2014**, *14*, 1515-1519

[5] Ting, D. Z-Y.; Chang, Y-C. L-Valley-Derived States in (001) GaSb/AlSb Quantum Wells and Superlattices, *Phys. Rev. B* **1988**, *38*, 3414

[6] Ikonić, Z.; Inkson, J. C.; Srivastava, G. P. On Level Splitting by Intervalley Interference Effects in Semiconductor Quantum Wells, *Solid State Commun.* **1990**, *76*, 117-119

[7] Herrera-Gomez, A.; Bravo-Sanchez, M.; Ceballos-Sanchez, O.; Vazquez-Lepe, M. O. Practical Methods for Background Subtraction in Photoemission Spectra, *Surf. Interface Anal.* **2014**, *10-11* 897-905

[8] Yeh, J. J.; Lindau, I. *At. Data Nucl. Data Tables*, **1985**, *32*, 1-55

[9] Tanuma, S.; Powell, C. J.; Penn, D. R. Calculations of Electron Inelastic Mean Free Paths III, *Surf. Interface Anal.* **1991**, *17* 927-939

[10] Powell, C. J.; Jablonski, A. NIST Electron Inelastic-Mean-Free-Path Database - Version 1.2, National Institute of Standards and Technology **2010**.